XLVI CILAMCE
VITÓRIA - ES - BRAZIL - 2025
XLVI IBERO-LATIN AMERICAN CONGRESS ON COMPUTATIONAL METHODS IN ENGINEERING

ANALYSIS OF ELECTROMAGNETIC PARAMETERS IN A THREE-PHASE INDUCTION MOTOR VIA NUMERICAL METHOD

Alana C. Carpanedo[1], Gustavo A. Lima[1], Werley G. Facco[1]

[1]*Federal Institute of Espírito Santo (IFES) – São Mateus Campus*
BR Norte Highway, Km 58, Litorâneo Neighborhood, São Mateus, 29932-540, Espirito Santo, Brazil
camatacarpanedoalana@gmail.com.br, 2001gustavoalves@gmail.com, werleyfacco@ifes.edu.br

Abstract. This work presents an exploratory analysis of a three-phase induction motor with a squirrel cage rotor using the Finite Element Method (FEM). The adopted geometry was based on the Tesla Model S design and discretized into a two-dimensional mesh. The governing equations were formulated based on the approach proposed by Arkkio [1], considering the magnetic vector potential under steady-state harmonic conditions. Electromagnetic properties were assigned according to values found in the literature, and the simulations were implemented in the MATLAB environment. The results include the distribution of the magnetic vector potential, the effective magnetic flux density, and the estimated torque. A convergence analysis based on mesh refinement was also carried out, demonstrating the consistency of the numerical solution. The results confirm the effectiveness of the methodology for analyzing the performance of induction machines.

Keywords: Finite Element Method, Induction Motor, Electromagnetic Simulation.

1 Introduction

Numerical methods are widely employed in engineering to solve complex problems described by differential equations. Among them, the Finite Element Method (FEM) stands out for its versatility in structural, thermal, and electromagnetic analyses, enabling the discretization of continuous domains and the approximation of solutions through algebraic systems.

For applications in electrical engineering, FEM is particularly effective in analyzing electromagnetic phenomena in transformers, sensors, actuators, and especially rotating electrical machines. Its ability to handle complex geometries and a variety of materials makes it ideal for detailed modeling.

In this context, this work applies FEM to the modeling of three-phase induction motors with squirrel cage rotors, a configuration widely used in industry due to its robustness, low cost, and simple construction. According to Americo [2] and Umans [3], this type of motor accounts for approximately 75% of all motors installed in Brazil. The aim is to explore the distribution of the magnetic field, magnetic vector potential, and electromagnetic torque, contributing to a precise and well-founded approach for design and diagnostic studies.

2 Mathematical formulations

The mathematical formulation that describes electromagnetic phenomena in electrical machines is based on Maxwell's equations. However, the direct application of these equations to complex geometries, combined with the nonlinear behavior of ferromagnetic materials, makes analytical solutions impractical. Therefore, it is necessary to use numerical methods capable of solving coupled partial differential equations related to the magnetic flux density, winding currents, and rotor dynamics.

The electromagnetic problem modeled in this study, under steady-state harmonic conditions, is governed by the equation obtained in Arkkio [1], presented as eq. (1):

$$\nabla\times(\nu\,\nabla\times A)+j\omega\sigma A=\frac{\sigma}{L}\cdot U\cdot e_z \tag{1}$$

where A represents the z component of the magnetic vector potential (for 2D problems), ν is the magnetic reluctivity, σ the electrical conductivity, ω the angular frequency, L the length of the machine, e_z the unit vector in the z direction, and U the vector of applied voltages.

The motor domain (Fig. 1a) was discretized into triangular finite elements (Fig. 1b). Each FEM equation term is evaluated locally and then assembled into the global system. To accurately model a real machine, the electrical behavior of rotor bars and stator windings must be incorporated through circuit laws, ensuring consistency between the FEM-computed magnetic field and the machine's electrical circuits.

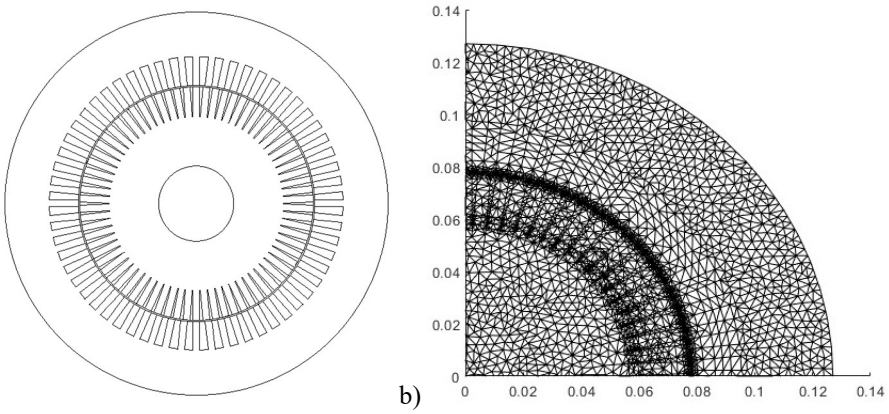


Figure 1. Tesla Model S' motor's: (a) Geometry (b) Finite element mesh with 10,849 nodes

In the case of rotor bars, modeled as conductors immersed in the magnetic field, a formulation proposed by Arkkio [1] is adopted, which relates the voltage U to the current I through the bar resistance R and the electromotive force induced by the magnetic vector potential A, taking into account the surface S of the conductor's cross-section, according to eq. (2):

$$U=R\cdot I+R\cdot j\omega\int_S \sigma A\cdot ds \tag{2}$$

To ensure consistency between the model and the machine's electrical behavior, current and voltage relationships in bars and coils are imposed based on Kirchhoff's Laws. Each stator conductor "i" carries a current "I_i" and is subjected to a voltage "U_i" while each rotor conductor "j" carries a "I_j" and a "U_j". The rotor bars are connected by end rings considered as ideal short circuits, as Arkkio [1], so that $U_j = U$ for all rotor conductors, where U is a constant, and the sum of rotor currents satisfies $\sum_{\{j=1\}}^{\{n_r\}} I_j = 0$, with n_r being the number of rotor bars. For the stator, the phase grouping follows the method proposed by Roças [4], neglecting end effects; thus, (I_i) is the same within a phase, and the sum of (U_i) equals the phase voltage. Kirchhoff's laws are applied to ensure charge conservation and account for potential drops across phase terminals. These relationships are coupled in the electromagnetic formulation for accurate machine representation. As a boundary condition, the Dirichlet condition $(A = 0)$ was applied to the outer surface of the machine in order to prevent the magnetic flux from crossing the boundary, as described by Arkkio [1] and Sarac and Stefanov [5].

The electromagnetic torque T is obtained from the simulation under steady-state harmonic conditions. The calculation was based on the Maxwell stress tensor method, with the formulation adapted from Arkkio [1], shown in eq. (3), through an integral approach:

$$T=\frac{1}{\mu_0(r_s-r_r)}\int_{Sag} r\,B_r\,B_\varphi\cdot ds \tag{3}$$

where μ_0 is the vacuum permeability, r_s and r_r are the outer and inner radii of the air gap respectively, S_{ag} is the cross-sectional area of the air gap, and B_r and B_φ are the radial and tangential components of the magnetic flux density.

In this study, the magnetic field acting on the induction motor is computed using the Finite Element Method, considering a two-dimensional simulation in which the magnetic vector potential A is oriented along the axial direction. The magnetic field B is obtained as the curl of A, as proposed by Arkkio [1].

3 Results and discussion

The geometric modeling of the Tesla Model S three-phase induction motor was developed based on the dimensions presented by Thomas et al. [6], as organized in the Tab. 1. The geometry was created in a two-dimensional environment using AutoCAD software, as shown in Fig. 1, adhering to the proportions and structural characteristics described.

Table 1. Rotor and stator parameters, in millimeters

Parameter	Stator	Rotor	Parameter	Stator	Rotor
Outer diameter	254.00	155.80	Tooth tip depth	1.00	-
Inner diameter	156.80	50.00	Slot Position	-	0.55
Slot depth	19.00	19.60	Tooth width	4.50	4.50
Slot opening width	2.90	-	Stack length	152.00	-
			Air gap	0.50	-

A 220 V, 60 Hz three-phase supply with 120° phase shifts was applied under a steady-state harmonic regime. Material properties were defined as in Table 2, representing typical induction motor materials: copper for windings, aluminum for the rotor, commercial iron for the core, and ferrosilicon for the rotor and stator laminated cores. Non-magnetic regions, such as air and windings, were modeled with permeability close to that of a vacuum.

Table 2. Physical Properties Assigned to the Model Subdomains

Subdomain	Electrical conductivity σ [S/m]	Magnetic permeability μ [H/m]
Air between rotor/stator	0	$\mu_0 = 4\pi \cdot 10^{-7}$
Windings (all phases)	$58 \cdot 10^6$	$0.999995 \cdot \mu_0$
Rotor bars	$35.5 \cdot 10^6$	$1.000021 \cdot \mu_0$
Core	0	$9000 \cdot \mu_0$
Rotor laminated core	0	$55000 \cdot \mu_0$
Stator laminated core	0	$55000 \cdot \mu_0$

Figures 2a and 2b show, respectively, the magnitude and phase angle of the magnetic vector potential A, obtained through FEM. The magnitude distribution, presented in Fig. 2a, highlights higher intensity in the air gap regions, where the magnetic field generated by the windings is concentrated. Fig. 2b illustrates the angular variation of A, in radians, associated with the phase shift among the three-phase currents. The continuous rotation pattern in the angle confirms the formation of the rotating field, a fundamental feature of induction motor operation, in which a 120° phase displacement produces a rotating magnetic vector responsible for the torque on the rotor, as described by Umans [3]. These results demonstrate the physical coherence of the obtained solution..

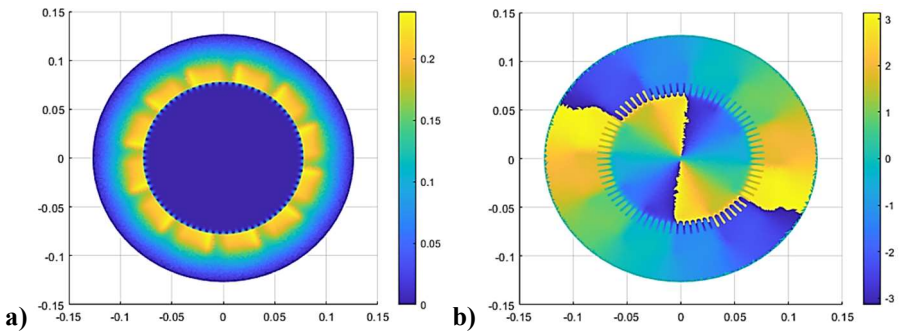


Figure 2. Distribution of the magnetic vector potential: (a) Magnitude of A [Wb/m]; (b) Phase angle of A

[radians]

Figure 3 illustrates the magnitude of the effective magnetic flux density B, obtained from the post-processing of the magnetic vector potential A. It can be observed that the highest values are concentrated near the air gap and the stator teeth regions, which aligns with the expected behavior for flux distribution in three-phase induction motors. This pattern is consistent with the literature, where the air gap acts as the main path for the magnetic flux linking the stator and rotor, as described by Umans [3]. The presence of well-defined flux channels indicates that the modeling of the coil excitation and the FEM solution were adequate. Furthermore, the observed spatial symmetry and the confinement of the flux within the conductive regions demonstrate a physically coherent electromagnetic response, reflecting the proper operation of the rotating field.

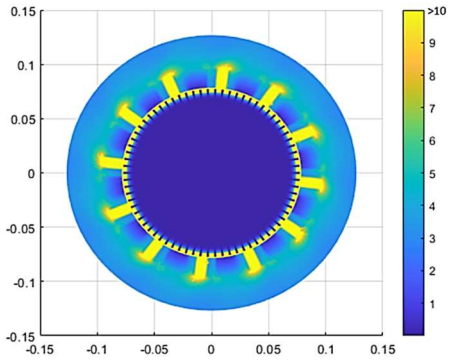


Figure 3. Magnitude of the magnetic flux density B [T]

Figure 4 shows the time variation of the electromagnetic torque obtained from the simulation under steady-state harmonic conditions. The calculation was based on the Maxwell stress tensor method, with the formulation adapted from Arkkio [1] through an integral approach. In this analysis, the rotor was considered locked relative to the stator, which corresponds to a slip value of $s = 1$. Under this condition, no mechanical rotation was modeled, and the torque represents the instantaneous electromagnetic interaction between the rotating stator field and the stationary rotor conductors. The primary purpose of this analysis was to confirm the dynamic electromagnetic behavior of the implemented model. A sinusoidal oscillatory behavior is observed, with a frequency corresponding to the applied supply, reflecting the periodic nature of the electromagnetic forces acting on the motor. The torque alternates between positive and negative values, indicating the interaction cycle between the stator's rotating field and the induced currents in the rotor - characteristic of induction motor operation. This profile is consistent with the expected outcome for a simulation with balanced three-phase supply and reinforces the consistency of the results obtained from the implemented model.

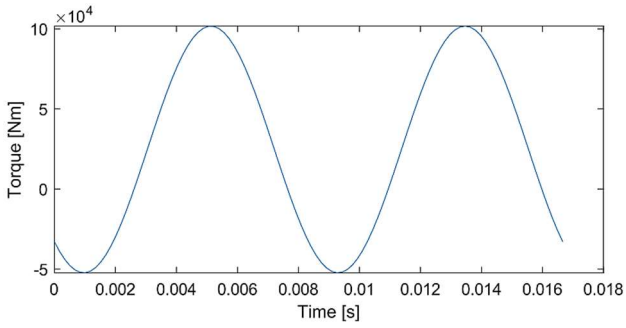


Figure 4. Electromagnetic torque over time

Finally, Fig. 5 shows the behavior of the relative error in the evaluation of the magnetic flux density B, utilizing first-order (linear) elements, as a function of mesh refinement, represented by the square root of the number of nodes n. Each point on the graph indicates the relative error of a specific mesh, taking as reference a

solution obtained with the finest mesh available, containing 678,974 nodes. A trend of error reduction is observed as the refinement increases, demonstrating the convergence of the numerical solution. Initially, the error decreases sharply, showing that coarse meshes present significant discrepancies compared to the more accurate solution. Beyond a certain level of refinement, the error stabilizes at very low values, indicating that the solution is sufficiently close to the reference solution.

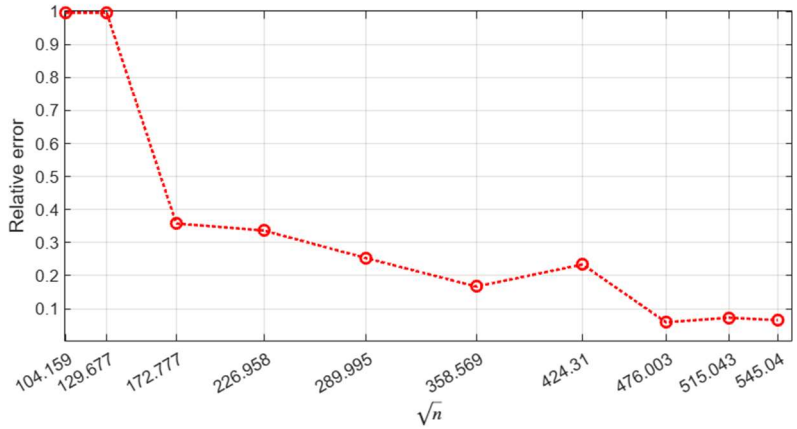


Figure 5. Relative error in the magnitude of B as a function of mesh refinement.

4 Conclusions

This study reinforces the effectiveness of the Finite Element Method (FEM) as an essential tool for the analysis of rotating electrical machines, such as induction motors. The graphical results provide a clear and detailed visual representation of the magnetic flux density distribution within the machine. These visualizations demonstrate the physical consistency of the obtained solution, showing flux concentration in the air gap and teeth, and confirming the formation of a rotating field - a fundamental characteristic for the operation of induction motors. In summary, the employed approach enables a deep understanding of the complex electromagnetic phenomena in electrical machines.

Acknowledgements. The authors acknowledge the Federal Institute of Espírito Santo, the agencies CNPq and CAPES, and FAPES for the financial support provided during the development of this study.

Authorship statement. The authors hereby confirm that they are the sole liable persons responsible for the authorship of this work, and that all material that has been herein included as part of the present paper is either theproperty (and authorship) of the authors

References

[1] A. Arkkio, *Analysis of Induction Motors Based on the Numerical Solution of the Magnetic Field and Circuit Equations*. Doctoral Thesis, Helsinki University of Technology, Espoo, Finland, 1987.
[2] M. Americo, *Sistemas Motrizes: Eficiência Energética e Técnicas de Acionamento*. PowerPoint presentations for the course Cepel/Sebrae-RJ/UFF, Niterói, Rio de Janeiro, Brazil, 2003.
[3] S. D. Umans, *Máquinas Elétricas de Fitzgerald e Kingsley*, 7th ed. AMGH Publishing, Porto Alegre, Rio Grande do Sul, Brazil, 2014..
[4] A. A. C. Roças. *Análise de Qualidade e Processos de Bobinagem de Motores de Indução de Baixa Tensão*. Undergraduate Thesis, Fundação Universidade Regional de Blumenau, Blumenau, Brazil, 2012.
[5] V. Sarac and G. Stefanov, 2011. *Calculation of Electromagnetic Fields in Electrical Machines using Finite Elements Method*. *International Journal of Engineering and Industries*, Vol. 2, No. 1.
[6] R. Thomas et al., *Modeling and design analysis of the Tesla Model S induction motor*, *IEEE Xplore*, 2020.